Commun Nonlinear Sci Numer Simulat 134 (2024) 108011

Contents lists available at ScienceDirect

Communications in Nonlinear Science and Numerical Simulation

journal homepage: www.elsevier.com/locate/cnsns

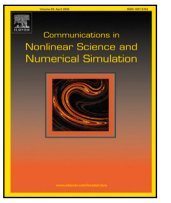

Research paper

Dynamics and scaling of internally cooled convection

Lokahith Agasthya *, Caroline Jane Muller

Institute of Science and Technology Austria, Am Campus 1, Klosterneuburg, 3400, Austria

ARTICLE INFO

Keywords:
Thermal convection with internal heat source
Radiative cooling
Atmospheric boundary layer flows
Linear Stability analysis

ABSTRACT

Our goal is to investigate fundamental properties of the system of internally cooled convection. The system consists of an upward thermal flux at the lower boundary, a mean temperature lapse-rate and a constant cooling term in the bulk with the bulk cooling in thermal equilibrium with the input heat flux. This simple model represents idealised dry convection in the atmospheric boundary layer, where the cooling mimics the radiative cooling to space notably through longwave radiation. We perform linear stability analysis of the model for different values of the mean stratification to derive the critical forcing above which the fluid is convectively unstable to small perturbations. The dynamic behavior of the fluid system is described and the scaling of various important measured quantities such as the total vertical convective heat flux and the upward mass flux is measured. We introduce a lapse-rate dependent dimensionless Rayleigh-number Ra_γ that determines the behavior of the system, finding that the convective heat-flux and mass-flux scale approximately as $\mathrm{Ra}_\gamma^{0.5}$ and $\mathrm{Ra}_\gamma^{0.7}$ respectively. The area-fraction of the domain that is occupied by upward and downward moving fluid and the skewness of the vertical velocity are studied to understand the asymmetry inherent in the system. We conclude with a short discussion on the relevance to atmospheric convection and the scope for further investigations of atmospheric convection using similar simplified approaches.

1. Introduction

The study of thermal, convective systems has a long history going back to the late 19th century, with the recorded observations of James Thomson [1] and the systematic experiments performed by Henri Bénard [2] setting the stage for further investigation into the effects of heating a fluid. Lord Rayleigh was the first to analytically describe the convective instability resulting from heating a fluid from below [3] using a model system that was named Rayleigh–Bénard (R–B) convection and one that has become the bedrock of studies on the behavior of thermal fluids and phenomena such as pattern formation, transition to chaos etc. [4,5]

One of the primary motivations to study R–B convection and other similar model fluid systems is to understand and characterise the behavior of the Earth's atmosphere. The atmospheric circulation of the earth is driven primarily by the heating of the earth's surface by the sun, which in turn heats the lowest level of the atmosphere. In addition to simple thermal effects, atmospheric convection includes a large number of physical, chemical and biological processes at different scales [6]. The study of atmospheric convection is usually performed by solving a large set of coupled non-linear equations which represent all these processes. These could be General Circulation Models (GCM) at the global scale [7,8] or Cloud Resolving Models (CRM) at smaller scales [9]. While they show realistic behavior, their complexity, especially the large number of state variables in the models makes their results hard to interpret and can even obscure a more fundamental understanding of atmospheric processes.

In the context of atmospheric convection, moist convection (ie., convection in the presence of moisture) is one of the most important phenomenon in the tropics. Here, the release of latent heat due to phase changes in water is very important to the

* Corresponding author.
E-mail address: lnagasthya@gmail.com (L. Agasthya).

https://doi.org/10.1016/j.cnsns.2024.108011
Received 6 November 2023; Received in revised form 5 March 2024; Accepted 2 April 2024
Available online 4 April 2024

dynamics, while the micro-physical details of the nature, number and size of hydrometeors (water in liquid or solid form) have an important feedback on the convective scale dynamics. Recently several studies have focused on developing simplified models which ignore several processes at various scales but capture essential features of the real atmosphere — for some examples, see [10–12]. These studies considered moist convection with highly simplified cloud microphysics, moist convection with varying thermal boundary conditions and moist-convection without considering the dynamics of liquid water respectively. They found robust evidence of an up-down asymmetry (where hot, rising updrafts occupy a smaller fraction of the domain than cold, subsiding air) and scalings with different parameters for important measured quantities such as the heat-flux, the mass flux in clouds, the height of maximum cloud formation, etc. Further exploration of such simplified convective models with some basic processes of the atmosphere represented while omitting or greatly simplifying other processes has the potential to uncover which are the fundamental processes which set the dynamics of tropical moist convection and which do not greatly affect the behavior of moist convection.

In this study, we focus on the simpler case of dry convection which occurs in the atmosphere when moisture is either absent or present in small enough quantities that condensation or freezing can be neglected. In other words, we consider convection of dry air or of moist air (i.e. with water vapor), but without phase change of water vapor into liquid or ice. For simplicity we will derive the equations for dry air, but we note that water vapor could easily be accounted for by replacing temperature with virtual temperature [6]. Dry convection occurs in the region between the earth's surface and the cloud-base, known as the sub-cloud layer. Dry convection is prevalent in the tropics over dry land and is particularly important in studies of the planetary boundary layer. Here, the constant cooling of the atmosphere by the emission of longwave radiation plays a non-negligible role in the dynamics.

To study this convective boundary layer, an idealisation that is most often made is to study the model fluid system with a fixed temperature at the lower boundary and (unlike Rayleigh–Bénard convection) a constant rate of diabatic cooling everywhere in the domain. An account of the global-heat balance and scaling of the heat-flux for this system can be found in Chapter 3.6 of [6], while the results from more recent simulations are reported in [13].

Berlengiero et al. in their study [14] (henceforth referred to as B2012) investigated the convective behavior of a layer of fluid with a fixed heat-flux at the lower surface and a uniform bulk-cooling term to understand the basic features of atmospheric dry convection with a constant radiative cooling to space. They argued that in some scenarios, particularly over land, fixed-flux boundary conditions are a better representation of the heating of the atmosphere by the surface than fixed temperature. The system consists of a layer of a Boussinesq fluid with a fixed input heat-flux f_0 at the lower surface, no vertical heat-flux at the upper boundary, a constant bulk-cooling $-R$ and a set adiabatic temperature lapse rate γ. The heat input into the system and the cooling via the bulk-cooling term must be in global balance to ensure that a system at thermal equilibrium is achieved.

In B2012, the authors described the dynamics of two different 3D flows, one with a non-zero, finite temperature stratification γ and a second flow with no stratification. The results presented included the vertical temperature profile for both cases, the volume fraction of the domain occupied by updrafts and the skewness of the vertical velocity. In particular, it was found that for both cases, less than half the volume was occupied by upward velocities, with concentrated intense hot plumes and large regions of subsiding flow. It was also found that the flow with $\gamma = 0$ showed strong clustering of hot plumes due to the interaction between the rising plumes and the returning subsiding flow from the upper boundary.

In the absence of a mean stratification ($\gamma = 0$ case), this set-up is equivalent and dynamically identical to other well-studied models of convection. Here we highlight the works of Goluskin [15,16] and the work conducted jointly by Aumaître, Gallet and others [17–19]. Goluskin considered a system of internally heated convection balanced by a constant outward heat-flux at the top boundary with an insulating lower boundary. This system is the same as the B2012 system after the transformations $z \to -z$ and $T \to -T$. Goluskin carried out the linear stability analysis of the system and inferred the critical non-dimensional forcing (Rayleigh number) for which the system is unstable to small perturbations. The works of Aumaitre, Gallet et al. consider a column of fluid that is cooled internally and heated internally. While the internal cooling extends throughout the domain, the heating extends from the lower surface up to a given typical height h. When $h \to 0$, this is identical to a fixed thermal-flux boundary condition. They characterised the convective transport, the flow and plume patterns and the nature of the boundary layer for varying h, finding that depending on whether the heating is localised in the boundaries ($h \to 0$) or more spread across the domain (h larger than typical height of the boundary layer), different regimes of turbulent transport are achieved.

In the presence of stratification (γ non-zero), the situation is more complicated given that the fluid instability extends only up to a finite height in the domain [14], with a layer of stable fluid over a layer of unstable fluid. This is the so-called "capping inversion" that occurs in the atmosphere on fair-weather days where the well-mixed atmospheric boundary layer is capped by a layer of statically stable air [20]. In the ice-water system [21], the non-linear temperature dependence of the density of water also leads to such a stability configuration.

In this study, we continue and expand the exploration of the internally cooled system introduced in B2012 for a wide-range of parameters, with the goal to derive scalings for important physical quantities and identify different behaviors as a function of key adimensional parameters. We begin by defining the Rayleigh number for the system and performing linear stability analysis to identify the critical Rayleigh number and the most unstable mode at this critical Rayleigh number. We discuss the relevance of the model to dry atmospheric convection. We characterise the changes in various important response parameters, particularly the temperature profiles, the up-down asymmetry and the total convective heat flux as well as the convective mass flux change with changing input parameters of the model.

The article is laid out as follows. Section 2 discusses the basic equations of our model, a recap of the basic relations derived in B2012 and a description of the numerical methods. In Section 3 we derive some more analytical results, define appropriate length, velocity and temperature scales to derive the non-dimensional parameters characterising the system and end with a discussion on typical values for various parameters in the atmosphere. Section 4 presents the linear-stability analysis for the system and the main results from our numerical simulations, following which we conclude with a discussion on the significance of the results as well as avenues for future work in Section 5.

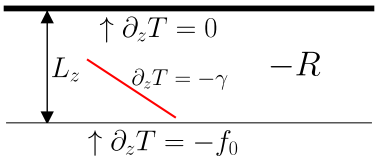

Fig. 1. Schematic of the model set-up. The internal cooling R is constant everywhere in the domain and is in large-scale balance with the incoming heat-flux f_0 at the lower boundary while the upper boundary is insulating. The fluid has a constant temperature lapse-rate γ.

2. Methodology: Equations and numerical simulations

2.1. Equations

As in B2012, we start with the incompressible Boussinesq [22] fluid equations along with the heat equation with a bulk-cooling term. We thus write the density as the sum of a reference constant density ρ_{ref} and a perturbation from this reference density denoted by ρ' such that $\rho = \rho_{ref} + \rho'$, with corresponding pressure $p = p_{ref}(z) + p'$ where $p_{ref}(z)$ is in hydrostatic balance with ρ_{ref} so that $dp_{ref}/dz = -\rho_{ref} g$. The equations for the total fluid velocity vector $\boldsymbol{u}$ with vertical component w and temperature fluctuations T' about a reference temperature T_{ref} are

$$\boldsymbol{\nabla} \cdot \boldsymbol{u} = 0, \tag{1}$$

$$\partial_t \boldsymbol{u} + (\boldsymbol{u} \cdot \boldsymbol{\nabla})\boldsymbol{u} = -(1/\rho_{ref})\boldsymbol{\nabla} p' + \nu \nabla^2 \boldsymbol{u} - \beta T' \boldsymbol{g}, \tag{2}$$

$$\partial_t T' + \boldsymbol{u} \cdot \boldsymbol{\nabla} T' + \gamma w = \kappa \nabla^2 T' - R, \tag{3}$$

where ν is the kinematic viscosity, β is the thermal expansion coefficient, $\boldsymbol{g} = -g\hat{z}$ is the acceleration due to gravity and $\gamma = g/c_p$ is the lapse-rate of the mean stratification (or the dry adiabatic lapse-rate, see Appendix A). The form of the equations above with the lapse-rate and the Boussinesq approximation was demonstrated first in [23]. R (> 0) is the bulk-cooling term applied to the fluid. As discussed by B2012, the term R breaks the up-down symmetry of the internally cooled system, leading to downward moving fluid ($w < 0$) occupying more than half the domain.

Here we have assumed that the density perturbation ρ' is given by $\rho'(T') = -\rho_{ref}\beta T'$, ρ_{ref} being the density of the fluid at temperature T_{ref}. For the Boussinesq approximation, it is only important that T' remains small enough that $\rho'(T')/\rho_{ref} \ll 1$ or equivalently, $\beta T' \ll 1$. For simplicity, we henceforth drop the primes and investigate Eqs. (1)–(3) without the primes.

The velocity and the temperature fields are periodic in the horizontal directions. At the bottom ($z = 0$) and top ($z = L_z$) surfaces, they are given by

$$\boldsymbol{u}(z = 0) = \boldsymbol{u}(z = L_z) = 0 \tag{4}$$

and

$$\left.\frac{\partial T}{\partial z}\right|_{z=0} = -f_0, \qquad \left.\frac{\partial T}{\partial z}\right|_{z=L_z} = -f_1. \tag{5}$$

It is noteworthy that this system is invariant under the transformation $T \to T + \delta T$ where δT is some constant temperature since the heat equation as well as the boundary conditions contain only derivative terms of the temperature. In moist convection, this is no longer true as the partition of water into solid, liquid and gaseous phases strongly depends on the precise thermodynamic temperature.

In addition to the fluid equations, we recall from B2012 that the large-scale thermal balance for the system, which can easily be derived by taking the domain average of Eq. (3) in steady state, is given by

$$\kappa(f_0 - f_1) = RL_z. \tag{6}$$

As in B2012, we set f_0 to be positive and $f_1 = 0$, leading to a balance between the radiative cooling in the domain and the net heat-flux from the bottom boundary. This also ensures that the average temperature of the domain remains stationary in time. Fig. 1 shows a schematic diagram of the fluid configuration.

A steady-state solution for the equations with $\boldsymbol{u} = 0$ everywhere leads to a temperature gradient

$$\frac{dT}{dz} = -f_0\left(1 - \frac{z}{L_z}\right) \tag{7}$$

with the corresponding temperature profile given by

$$T(z) = T_{bot} - zf_0\left(1 - \frac{z}{2L_z}\right), \tag{8}$$

where T_{bot} is the temperature at $z = 0$. The fluid is stably stratified where $\partial_z T > -\gamma$, which is given by $z > L_z(1 - \gamma/f_0)$. Thus we expect that when convection occurs, it occurs only up to a height z_0 given by

$$z_0 = L_z(1 - \gamma/f_0). \tag{9}$$

It should be noted here that the equations may also be written in terms of a potential temperature $\theta \equiv T + \gamma z$. This would eliminate the adiabatic cooling term γw with the boundary conditions given by $\partial_z \theta = -f_0 + \gamma$ and $\partial_z \theta = \gamma$ at the lower and top surfaces respectively. Hence, the stratified system is equivalent to an unstratified fluid with fixed-flux temperature conditions at both boundaries.

2.2. Numerical methods

In order to understand and investigate the behavior of the above system, we solve the system of Eqs. (1)–(5) numerically in a 2D domain box with fixed aspect ratio 2π which is periodic in the horizontal direction. The various input parameters other than the extent of the domain are γ, κ, ν, the product βg and f_0. f_1 is set to 0, ρ_{ref} to unity while $R = \kappa f_0 / L_z$ in accordance with the condition of thermal equilibrium (Eq. (6)). We also perform simulations for a horizontally periodic 3D domain with the same aspect ratio for a few selected parameters. The equations are solved with a python code employing the Dedalus spectral solver [24], using Fourier components in the periodic horizontal directions and Chebyshev polynomial decomposition for the vertical direction. The equations are solved on a 256×128 grid for most flows, with the resolution rising to 2048×1024 for the most strongly forced flows. All 3D flows were solved on a $256 \times 256 \times 128$ grid. The code was bench-marked against the results from B2012.

The outputs of the simulations are analyzed to calculate various flow parameters only after the flow has become statistically stationary, wherein the average kinetic energy and the average temperature of the domain as well as the average temperature at the top and bottom surfaces of the domain fluctuate about a constant value. While we report only a few measurements from 3D runs, we have checked that all the below results are qualitatively true for 2D as well as 3D flows, unless otherwise mentioned.

3. Model overview

3.1. Exact relations

In addition to the large-scale thermal balance and the steady-state temperature profile (Eqs. (6) and (8)), we also derive the z-dependent thermal balance as is standard in the case of Rayleigh–Bénard convection and other model thermal fluid systems. Rewriting the advective term in flux-form ($\boldsymbol{\nabla} \cdot (\boldsymbol{u} T)$) and integrating the horizontal statistical average of Eq. (3) from the bottom to a height z gives

$$\langle wT \rangle_{A,t} - \kappa \langle \partial_z T \rangle_{A,t} = R(L_z - z), \tag{10}$$

where $\langle \cdot \rangle_{A,t}$ indicates the statistical average taken at a fixed height z and we have used the fact that in the steady-state, the time-derivatives go to 0 while horizontal derivatives of the flux term average out to zero due to the periodic boundary conditions. This relation shows that the total vertical heat transfer by convection decays linearly as a function of height. Heat is removed uniformly at each height by the bulk radiative cooling term. In case of f_1 not being set to 0, there would be an addition term κf_1 on the RHS which represents the outward heat-flux at the top of the domain.

For our system, we also calculate the global thermal dissipation $\epsilon_T \equiv \kappa \langle |\boldsymbol{\nabla} T|^2 \rangle$ given by (see Appendix B.1)

$$\begin{aligned} \kappa \langle |\boldsymbol{\nabla} T|^2 \rangle &= \frac{\kappa}{L_z} T_{bot} f_0 - \gamma \langle wT \rangle - R \langle T \rangle \\ &= R \langle T_{bot} - T \rangle - \gamma \langle wT \rangle. \end{aligned} \tag{11}$$

where $\langle \cdot \rangle$ indicates the statistical average taken over the whole domain and T_{bot} is the measured average temperature at $z = 0$. We can see that the RHS value still remains invariant under the transformation $T \to T + \delta T$. The strength of the thermal gradients in the fluid increases with the average departure of the domain temperature from T_{bot} and decreases when convective transfer of heat is efficient, that is $\langle wT \rangle$ is large.

The viscous dissipation $\epsilon \equiv (\nu/2) \sum_{i,j} (\partial u_i / \partial x_j + \partial u_j / \partial x_i)^2$ is given by (see Appendix B.2)

$$\frac{\nu}{2} \sum_{i,j} \left(\frac{\partial u_i}{\partial x_j} + \frac{\partial u_j}{\partial x_i} \right)^2 = \beta g \langle wT \rangle. \tag{12}$$

We can see that, similar to the Nusselt number in R–B convection, the response quantity $\langle wT \rangle$ is of fundamental importance and it determines the convective heat transfer properties of the fluid system as well as the strength of the thermal and kinetic gradients. In the context of a convecting atmosphere, this value is the vertical buoyancy-flux, crucial in determining the thermodynamics of the atmosphere in shallow dry convection. In deep, moist convection too, the thermal flux in the sub-cloud layer is of crucial importance — for example it is approximately equal to the pressure-work done by the fluid and this is closely related to the production of irreversible entropy in the sub-cloud layer [25].

Analogous to the usual definition for R–B convection we define the Nusselt number Nus for the current system as

$$\text{Nus} = \frac{\langle wT \rangle}{\kappa T_0 / L_z} \tag{13}$$

where T_0 is a temperature scale of the system to be defined later. The Nusselt number here is thus a non-dimensionalised heat-flux. The Nusselt number here compares the vertical heat-flux with the typical conductive heat flux. When the flow is conductive, we have no fluid motion and hence Nus = 0. In the presence of convection, Nus has a finite value which increases with the increase in the strength of convection.

3.2. Non-dimensional parameters

3.2.1. Buoyancy scaling

To quantify the system and non-dimensionalise the equations, we need appropriately defined temperature, velocity and length scales. Since the dynamics of the system is set by the bulk-cooling R, which has SI unit dimensions of Kelvin s^{-1}, we can write the temperature scale T_0 as

$$T_0 = Rt_0 \tag{14}$$

where t_0 is the appropriate time-scale, with length-scale L_z giving the velocity scale $U_0 = L_z/t_0$. As is standard for thermal flows, we write U_0 as a convective velocity given by

$$U_0 = \sqrt{\beta g T_0 L_z}. \tag{15}$$

Combining the above equations gives finally

$$T_0 = (\beta g)^{-1/3} R^{2/3} L_z^{1/3}, \tag{16}$$

$$U_0 = (\beta g)^{1/3} R^{1/3} L_z^{2/3}, \tag{17}$$

$$t_0 = (\beta g)^{-1/3} R^{-1/3} L_z^{1/3}. \tag{18}$$

Using these scales, the equations are non-dimensionalised as

$$\widehat{\boldsymbol{\nabla}} \cdot \widehat{\boldsymbol{u}} = 0, \tag{19}$$

$$\partial_{\hat{t}} \widehat{\boldsymbol{u}} + (\widehat{\boldsymbol{u}} \cdot \widehat{\boldsymbol{\nabla}}) \widehat{\boldsymbol{u}} = -\widehat{\boldsymbol{\nabla}} \widehat{p} + \sqrt{\frac{\mathrm{Pr}}{\mathrm{Ra}}} \widehat{\nabla}^2 \widehat{\boldsymbol{u}} + \widehat{T} \hat{z}, \tag{20}$$

$$\partial_{\hat{t}} \widehat{T} + \widehat{\boldsymbol{u}} \cdot \widehat{\boldsymbol{\nabla}} \widehat{T} + (\gamma/f_0) \sqrt{\mathrm{Pr\,Ra}} \widehat{w} = \frac{1}{\sqrt{\mathrm{Pr\,Ra}}} \widehat{\nabla}^2 \widehat{T} - 1, \tag{21}$$

where the hat ($\widehat{\ }$) indicates the non-dimensionalised variable or operator obtained by dividing by the appropriate dimensional scale. The non-dimensional parameters are the Rayleigh-Number Ra, the Prandtl number Pr and the ratio γ/f_0 between the lapse-rate and heat-flux. The Rayleigh number is given by

$$\mathrm{Ra} = (\beta g)^{2/3} \frac{R^{2/3} L_z^{10/3}}{\nu \kappa}. \tag{22}$$

This is equivalent to the form derived in B2012, albeit without appealing to a flux formulation. This equivalence is not surprising as the approach of B2012 (setting the time-scale of the fluid motion equal to the time-scale of radiative cooling) is identical to our approach in setting the temperature scale according to the rate of radiative cooling, which gives a non-dimensional rate of radiative cooling ($RL_z/(U_0 T_0)$) of unity. Ra can also be re-written in terms of f_0 using $R^{2/3} L_z^{10/3} = (\kappa f_0)^{2/3} L_z^{8/3}$ from Eq. (6), which gives $\mathrm{Ra} \propto f_0^{2/3}/\kappa^{1/3}$.

The Prandtl number is the ratio ν/κ between the viscosity and the thermal conductivity. The ratio γ/f_0 sets the height z_0 above which the fluid is stably stratified (see Eq. (9)). It can indeed be argued that the height z_0 rather than L_z is the appropriate length scale to define the convective time and velocity-scales, which leads to a lapse-rate dependent Rayleigh number Ra_γ given by

$$\mathrm{Ra}_\gamma = (\beta g)^{2/3} \frac{R^{2/3} z_0^{10/3}}{\nu \kappa} = \mathrm{Ra} \left(1 - \frac{\gamma}{f_0}\right)^{10/3}. \tag{23}$$

In this study, we solve the system of equations in arbitrarily chosen simulations units — however, all the results presented involve only non-dimensional quantities and it is the scaling with the non-dimensional parameters that we are interested in to characterise the system.

While several of our simulations have large differences of temperature between the lower and upper surface, thus invalidating the assumptions underlying the Boussinesq approximation, we note that this temperature difference is dictated by a combination of the temperature gradient at the lower boundary f_0 and the lapse-rate γ. The principle of dynamic similarity for flows with the same Ra_γ can be used to construct an equivalent flow with f_0 chosen to be an appropriately small value and also decreasing κ and ν to retain the same Ra_γ ($\propto f_0^{2/3}/\kappa^{1/3}$).

3.2.2. Diffusive scaling

It is also standard to define the velocity scale as a diffusive velocity U_D given by

$$U_D = \kappa/L_z. \tag{24}$$

Defining the diffusive time-scale t_D as L_z/U_D and again setting R to be unity, gives the non-dimensional equations

$$\widehat{\boldsymbol{\nabla}} \cdot \widehat{\boldsymbol{u}} = 0, \tag{25}$$

$$\partial_{\hat{t}} \widehat{\boldsymbol{u}} + (\widehat{\boldsymbol{u}} \cdot \widehat{\boldsymbol{\nabla}}) \widehat{\boldsymbol{u}} = -\widehat{\boldsymbol{\nabla}} \widehat{p} + \mathrm{Pr}\, \widehat{\nabla}^2 \widehat{\boldsymbol{u}} + \mathrm{Pr\,Ra}_D \widehat{T} \hat{z}, \tag{26}$$

$$\partial_{\hat{t}}\hat{T} + \hat{\boldsymbol{u}}\cdot\hat{\boldsymbol{\nabla}}\hat{T} + (\gamma/f_0)\hat{w} = \hat{\nabla}^2\hat{T} - 1, \tag{27}$$

where Ra_D is now the diffusive Rayleigh number, related to the buoyancy Rayleigh number as

$$\mathrm{Ra}_D = \mathrm{Ra}^{3/2}. \tag{28}$$

We refer the reader to [16] or [26] for a detailed derivation of the diffusive temperature, velocity and time-scales and the above non-dimensional equations.

We make use of the above non-dimensional equations with Ra_D for the linear stability analysis (§ 4.1) as it simplifies the algebra greatly and it has been used prominently by previous studies with fixed heat-flux boundary conditions for such stability analyses.

3.3. Some orders of magnitude

In the context of a typical scenario of dry convection in the tropics, convection occurs in a layer of atmosphere from the surface to cloud base level, which is 500 m to 3 km high, with the thermal heat flux (sensible heat flux) from the surface in the order of $10-100$ W m^{-2}, radiative cooling to space of $1-2$ K day^{-1} and dry air with a typical $\beta \sim 1/300$ K^{-1}.

Sensible heat flux in W m^{-2} can be converted to an equivalent thermal gradient by dividing by $(\rho\kappa c_p)$ where ρ is the density and c_p is the heat capacity of air. When we consider an eddy-diffusivity like value of thermal conductivity $\kappa \sim 10^{-2}$ m^{2}s^{-1}, with $\rho \sim 1$ kg m^{-3} and $c_p \sim 10^3$ J kg^{-1} K^{-1} we obtain $f_0 \sim \mathcal{O}(1)$. Considering the adiabatic lapse-rate to be the typical dry value of 0.01 K m^{-1} and $\beta g \sim 1/30$ m s^{-2}K^{-1} gives Ra_γ to be at the least of order 10^9. For the true molecular value of ν and κ, the value of Ra_γ would be closer to 10^{15}. It is important to note here that even for the lowest estimates of f_0, γ is less than 1% of f_0.[i]

Given that the value of 10 W m^{-2} for the sensible heat-flux is a global annual average, there do exist scenarios where the sensible heat flux can be far smaller than this value. However, in these situations it is unrealistic to model the atmosphere to be locally in equilibrium with radiative cooling — instead the energy balance would be determined by large-scale, horizontal heat-fluxes or the cooling term would dominate the heat-equation. Studies of adjustment in such an out-of-equilibrium state is beyond the scope of the current study.

In using the current system as a model for atmospheric dry-convection, it is also important to assess the validity of the Boussinesq-approximation for dry convection. For a layer of atmosphere around 1 km thick, temperature differences ΔT between the bottom and the top of this layer are of the order of $\sim$ 10 K , as the atmosphere remains close to a dry adiabatic profile. This translates to $\beta\Delta T \approx 3\times10^{-2}$. Thus, we see that the Boussinesq approximation remains an excellent approximation in the simulation of dry convection. In the presence of moisture and the ensuing deep, moist convection that penetrates up to the top of the troposphere ($\sim$ 15 km), the Boussinesq approximation breaks down and the vertical variation in density is significant.

From the above discussion it is clear that the current model under investigation is valid for shallow, sub-cloud dry convection where it can be assumed that the convection and sensible heat-flux is locally in equilibrium with the cooling of the atmosphere through outgoing long-wave radiation to space. We study flows with $\mathrm{Pr} = 1$ and Ra_γ up to 10^6. γ/f_0 is varied from 0 to 0.75, with the results of the simulations mainly presented for the values of $\gamma/f_0 = 0, 0.2, 0.4, 0.75$.

4. Results

4.1. Linear stability analysis

The procedure to find the critical Rayleigh number for a convective instability in a thermal fluid has been well established [3,27]. We consider the conductive state with $\boldsymbol{u} = 0$ and the temperature field varying only in the vertical according to Eq. (8). Now we consider a small perturbation in velocity and temperature given by $\boldsymbol{U} = (U, W)$ and H respectively. The non-dimensional equations of motion then become [15]

$$\boldsymbol{\nabla}\cdot\boldsymbol{U} = 0, \tag{29}$$

$$\partial_t\boldsymbol{U} = -\boldsymbol{\nabla}P + \mathrm{Pr}\,\nabla^2\boldsymbol{U} + \mathrm{Pr}\,\mathrm{Ra}_D H\hat{z}, \tag{30}$$

$$\partial_t H + (\gamma/f_0)W - (1-z)W = \nabla^2 H. \tag{31}$$

where P is the pressure perturbation with the stable temperature gradient absorbed. Here, the non-linear advective terms are neglected and the stable temperature profile enters the equations only via its derivative $(1-z)$. The boundary conditions on W and H at the top and bottom surfaces are given by

$$W\Big|_{z=0,1} = \partial_z W\Big|_{z=0,1} = 0; \partial_z H\Big|_{z=0,1} = 0. \tag{32}$$

The boundary conditions W arise from the no-slip velocity boundary condition (Eq. (4)) and the incompressibility condition respectively while the condition on H arises from the fact that for the fixed heat-flux, $\partial_z T$ at the boundaries is fixed and constrained by the large-scale heat-balance, meaning that there can be no local perturbations from this fixed flux value.

[i] If we consider real-world observations, it is well-known that ambient temperature measurements are recorded 2 metres above the land surface, which is typically a few Kelvin warmer than the air at the lowest level of the atmosphere on a sunny day. Thus, the temperature gradient at the boundary here is of the order of 1 Kelvin per metre, compared to the dry adiabatic lapse rate of 0.01 K m^{-1}.

The curl is applied twice ($\boldsymbol{\nabla}\times\boldsymbol{\nabla}\times$) to the momentum equation Eq. (30), the vertical component of which gives

$$\frac{1}{\mathrm{Pr}}\partial_t(\partial_z^2)W = \nabla^4\ W + Ra_D(\partial_x^2)H, \tag{33}$$

while the heat-equation is simplified to

$$\partial_t H = \nabla^2 H + (1-\gamma/f_0 - z)W. \tag{34}$$

In looking for marginally stable states that do not vary in time ($\partial_t \to 0$), the problem reduces to

$$\nabla^4 W = -\mathrm{Ra}_D\partial_x^2 H, \tag{35}$$

$$\nabla^2 H = -(1-\gamma/f_0 - z)W. \tag{36}$$

The critical Rayleigh number Ra_c for which the system is unstable to perturbations is given by the smallest Ra_D for which the system of Eqs. (35)–(36) has a real, non-zero solution. This eigenvalue problem can be decomposed into Fourier modes by considering the perturbations to have the form

$$W = \mathcal{W}(z)e^{ikx}, \tag{37}$$

$$H = \mathcal{H}(z)e^{ikx}, \tag{38}$$

where k is the horizontal wavenumber of the disturbance. This leads to

$$\left(\frac{d^2}{dz^2} - k^2\right)^2 \mathcal{W} = \frac{d^4\mathcal{W}}{dz^4} - 2k^2\frac{d^2\mathcal{W}}{dz^2} + k^4\mathcal{W} - = k^2\mathrm{Ra}_D\mathcal{H}, \tag{39}$$

$$\frac{d^2\mathcal{H}}{dz^2} - k^2\mathcal{H} = -(1-\gamma/f_0 - z)\mathcal{W}. \tag{40}$$

For the equivalent case of uniformly heated convection with a constant outward heat-flux at the top, the solution to the above eigenvalue problem without stratification ($\gamma/f_0 = 0$) is found by considering the long-wavelength asymptote, ie., the limit $k \to 0$. We will first derive the $k \to 0$ critical Rayleigh number and will see that it indeed yields the most unstable mode for weak stratification. We will then extend the results to finite stratification, which instead occurs at non zero wavenumber $k_c \neq 0$.

4.1.1. Long-wavelength solution for weak stratification

Focusing here on the $k = 0$ limit, the expansion in k^2 of the form

$$\mathcal{W} = \mathcal{W}_0 + k^2\mathcal{W}_2 + k^4\mathcal{W}_4 + \dots, \tag{41}$$

$$\mathcal{H} = \mathcal{H}_0 + k^2\mathcal{H}_2 + k^4\mathcal{H}_4 + \dots, \tag{42}$$

yields

$$\mathcal{W}_0 = 0; \quad \mathcal{H}_0 = 1; \quad \frac{d^4\mathcal{W}_2}{dz^4} = \mathrm{Ra}_c\mathcal{H}_0; \quad \frac{d^2\mathcal{H}_2}{dz^2} - \mathcal{H}_0 = -(1-\gamma/f_0 - z)\mathcal{W}_2. \tag{43}$$

where Ra_c is the critical Ra_D for transition to convection. Since $\mathcal{H}_0$ is a constant and the 4th-derivative of $\mathcal{W}_2$ is a constant, $\mathcal{W}_2$ must be given by

$$\mathcal{W}_2 = Ra_c P^{(4)}(z), \tag{44}$$

where $P^{(4)}(z)$ is a 4th-order polynomial in z with the coefficients to be determined from the boundary conditions given in Eqs. (32). Requiring that each of the $\mathcal{W}_i, \mathcal{H}_i$ follow the same boundary conditions as W and H respectively, yields

$$P^{(4)}(z) = \frac{1}{24}(z^4 - 2z^3 + z^2). \tag{45}$$

Integrating the right-most equation of (43) from the limits 0 to 1 and noting that $\mathcal{H}_0 = 1$, $d_z\mathcal{H}\big|_{z=0,1} = 0$ leads to

$$1 = \frac{Ra_c}{24}\int_0^1 (1-\gamma/f_0 - z)(z^4 - 2z^3 + z^2)dz \tag{46}$$

after substituting for $\mathcal{W}_2$ from Eqs. (44) and (45). Finally, we derive the expression for the critical diffusive Rayleigh number as

$$\mathrm{Ra}_c = \frac{24}{\int_0^1 (1-\gamma/f_0 - z)(z^4 - 2z^3 + z^2)dz} = \frac{1440}{1 - 2\gamma/f_0}. \tag{47}$$

We note here that all of the above analysis has been performed by Goluskin [15,16] with $\gamma = 0$. While Goluskin considered an internally heated system with $\partial_z T > 0$ for the conductive profile, leading to $-zW$ instead of $-(1-z)W$ in the LHS of Eq. (31), this still leads to the same 4th order polynomial form for $\mathcal{W}_2$ and the final integral yields $\mathrm{Ra}_c = 1440$.

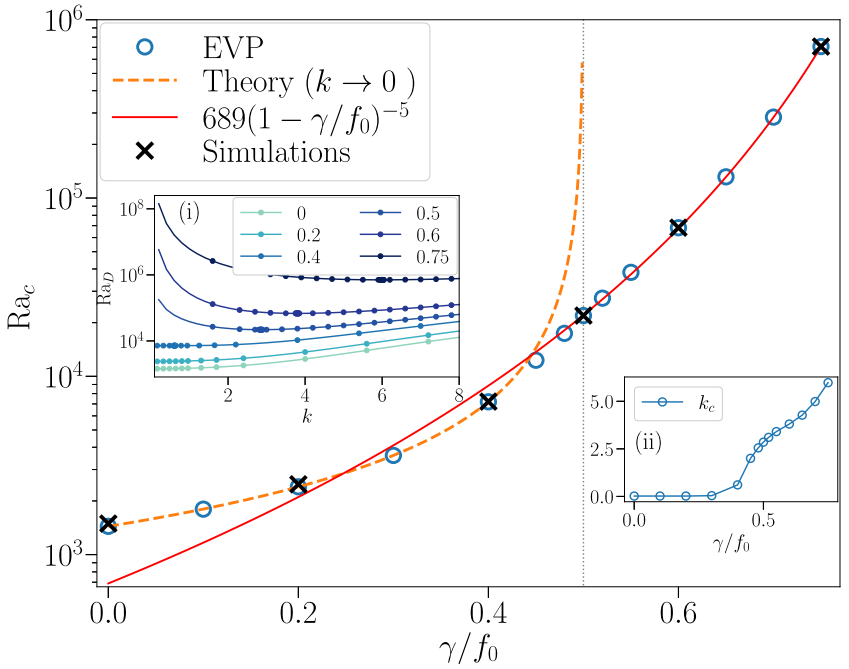

Fig. 2. Variation of the critical diffusive Rayleigh number Ra_c with γ/f_0. EVP values are obtained by solving the linear eigenvalue problem numerically using the EVP command of the python package Dedalus. Theory curve shows the long-wavelength asymptote, black crosses show the values inferred from full 2D simulations while the red solid line is an empirical best-fit assuming constant $Ra_\gamma = 689^{2/3}$. Inset (i) shows the wavenumber of the most unstable mode for the linear eigenvalue problem. Inset (ii) shows the eigenvalue Ra_D for varying k.

Table 1
Critical Ra_γ and diffusive Rayleigh number Ra_c for transition to convection. (S) indicates the value from 2D simulations. (EVP) indicates the numerical solution from solving the linear eigenvalue problem, ($k \to 0$) is the theoretical prediction from the long-wavelength asymptote while k_c is the least stable mode from the EVP calculation.

γ/f_0	Ra_γ (S)	Ra_c (S)	Ra_c (EVP)	Ra_c ($k \to 0$)	k_c
0	130.62	1492.87	1440.02	1440	0.02
0.2	87.07	2479.5	2399.86	2400	0.02
0.4	68.014	7213.5	7193.74	7200	0.606
0.5	77.7	21 915	21 904.4	∞	2.854
0.6	78.695	68 175	68 139.33	−7200	3.804
0.75	78.138	707 287.5	707 352.9	−2880	5.98

4.1.2. Non-zero wavenumber solution for stronger stratification

For $\gamma/f_0 > 0$, Ra_c from Eq. (47) increases, approaching ∞ for $\gamma/f_0 \to 0.5$. When $\gamma/f_0 > 0.5$, Ra_c is negative. Here, the small wavenumber (or long-wavelength) approximation is no longer valid as the mode of least stability does not approach the $k = 0$ mode. The mode of least stability is the value of wavenumber k for which the linear eigenvalue problem in Ra_D yields the smallest, real solution. We denote this wavenumber as k_c.

We use two approaches to infer the critical Ra_D for transition to convection in our system for varying γ/f_0. In the first approach, we use full 2D simulations as described in Section 2.2 and examine whether the flow shows any convective motion or remains conductive. The flow is initialised with a stable temperature profile with spatially varying random Gaussian noise. This leads to an initial spike in kinetic energy following which, the kinetic energy either falls to 0 (ie., extremely small values below 10^{-25} in the simulation units) or remains non-zero accompanied by a non-zero value for the convective heat-flux.

Secondly, we directly solve the linear eigenvalue problem described by Eqs. (39)–(40). This is achieved using the EVP (Eigenvalue Problem) class in the Dedalus Package, numerical details of which may be found in [24]. Formulations of such linear stability problem leading to similar eigenvalue equations have been considered previously for various problems. The most generalised formulation was provided in [26] for convection with a constant internal heat-source or sink and any combination of fixed-temperature or fixed-flux thermal boundary conditions at the top and bottom walls. The eigensystem was explicitly solved numerically only for the case of fixed temperature boundary conditions with an internal heat source. Other studies considered internally cooled system with fixed temperature at the lower boundary [13], internally heated convection with a varied combination of thermal boundary conditions [15,16], convection heated with a constant flux from below with no internal heat-source [28], compressible convection [29] and convection in the water-ice system where density varies non-linearly with temperature [21]. To

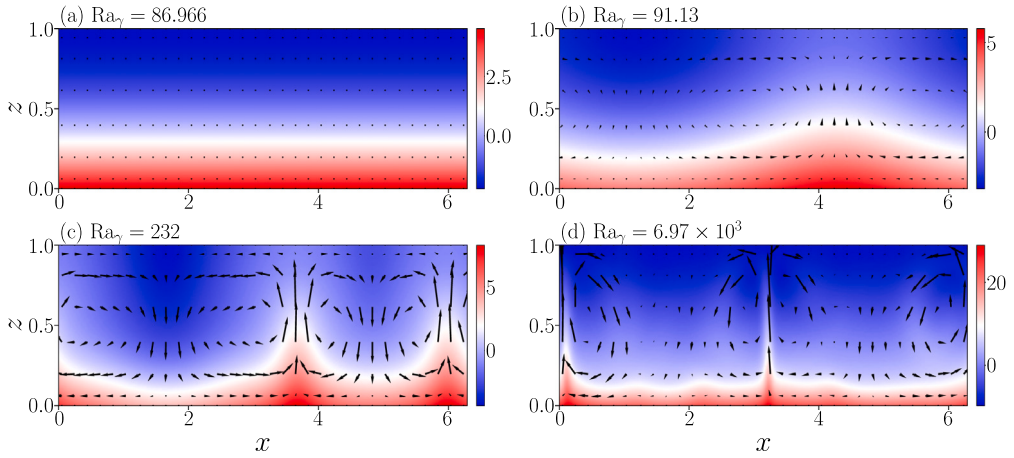

Fig. 3. Instantaneous snapshots of the temperature field T in the stationary regime for flows with different Ra_γ as indicated in the figure and $\gamma/f_0 = 0.2$. The temperature fields are divided by the respective temperature scale T_0 defined in Eq. (16) and scaled such their domain average is 0. Panel (a) shows a conductive state while panels (b), (c) and (d) show convective flows. The arrows represent velocity vectors with the arrow length in plot units equal to velocity magnitude divided by U_0, U_0, $2U_0$ and $5U_0$ respectively where U_0 is the velocity scale defined in Eq. (17).

the best of our knowledge, the solution to the linear stability eigenvalue problem for the current system has not been reported elsewhere in the literature, though the methods have been discussed.

The results are summarised in Fig. 2 and Table 1. The main figure shows that the long-wavelength asymptote (orange, dashed line) for the critical Rayleigh number for transition to convection is an excellent estimate up to $\gamma/f_0 \sim 0.4$ inferred through both, simulations (black crosses) and through solving the eigenvalue problem (empty blue circles) numerically. As γ/f_0 approaches the value of 0.5, indicated by the dotted gray vertical line, Ra_c from the simulations and the EVP theoretical solutions departs from this prediction. Instead, the values for larger γ/f_0 lie on the $(1-\gamma/f_0)^{-5}$ curve. This corresponds to a constant $\mathrm{Ra}_\gamma \approx 78$.

The insets of the figure show the behavior of the eigenvalue Ra_D for perturbations with varying wave-number k inferred from the EVP method. Inset (i) plots the eigenvalue Ra_D as a function of k for different values of γ/f_0. When $\gamma = 0$, the eigenvalue is a monotonically increasing function of k, consistent with the long wavelength instability. Upon increasing γ/f_0, the shape of the curve changes, with the value of Ra_D decreasing before reaching a minimum value and then increasing for larger k. For example, for $\gamma/f_0 = 0.4$, $k_c = 0.606$, with $Ra_c = 7193.74$, marginally smaller than the theoretical value of $\mathrm{Ra}_c = 7200$. Thus, the long-wavelength asymptote remains an excellent approximation even when only the lower 60% of domain height is unstably stratified.

As γ/f_0 is increased further, the value of k_c starts to significantly increase and the local minima in the curve starts to become more pronounced. This transition is apparent from comparing the $\gamma/f_0 = 0.4$ and $\gamma/f_0 = 0.5$ curves in inset (i). Now, the smallest wavenumber is no longer the most unstable mode, with k_c increasing to nearly 6 for $\gamma/f_0 = 0.75$.

Table 1 lists the numerical values for the critical Ra_γ and Ra_D found using full 2D fluid simulations. These are compared with the long-wavelength asymptote, the numerical EVP solution as well as the k_c found from the EVP procedure. These are the same as the plotted values, tabulated for more clarity.

4.2. Transition to convection

When Ra_γ is below the critical value, the fluid remains motionless. When Ra_γ (or equivalently, f_0) is increased, the flow becomes convective with convective rolls that extend up to height z_0. Fig. 3 shows instantaneous snapshots of the linearly scaled, non dimensionalised temperature field for 2D flows with $\gamma/f_0 = 0.2$. When the flow is stable (see panel (a)), the fluid is held motionless by viscosity and thermal dissipation and the temperature field is perfectly homogeneous in the horizontal direction. When f_0 is increased slightly, as in panel (b), the flow shows a pattern of large, space-filling convective rolls. Larger values of f_0 shown in the lower panels show intense and clearly defined rising convective plumes, where the hot, rising plumes have a large positive height-wise temperature anomaly, while the gently subsiding regions outside these plumes have a smaller negative height-wise temperature anomaly. In panel (d), the hot plume is the narrowest with the highest velocities (seen by length of the arrows) strongly concentrated in the rising plumes. The reader should note that the arrows representing the velocity fields are scaled by a different value in each panel only to ensure clarity in the figure — arrow lengths must not be used to compare the velocity between different panels.

4.3. Flow structures and profiles

In the convective regime, intense hot plumes arise from the lower surface along with broad regions of cold subsidence. There exists a small diffusive boundary layer near the lower surface underneath the intense hot plumes. Here, the vertical gradient of the temperature field ($\partial_z T$) quickly goes from $-f_0$ to $-\gamma$ as seen in Fig. 4(a). Above this layer lies a convective bulk region where the

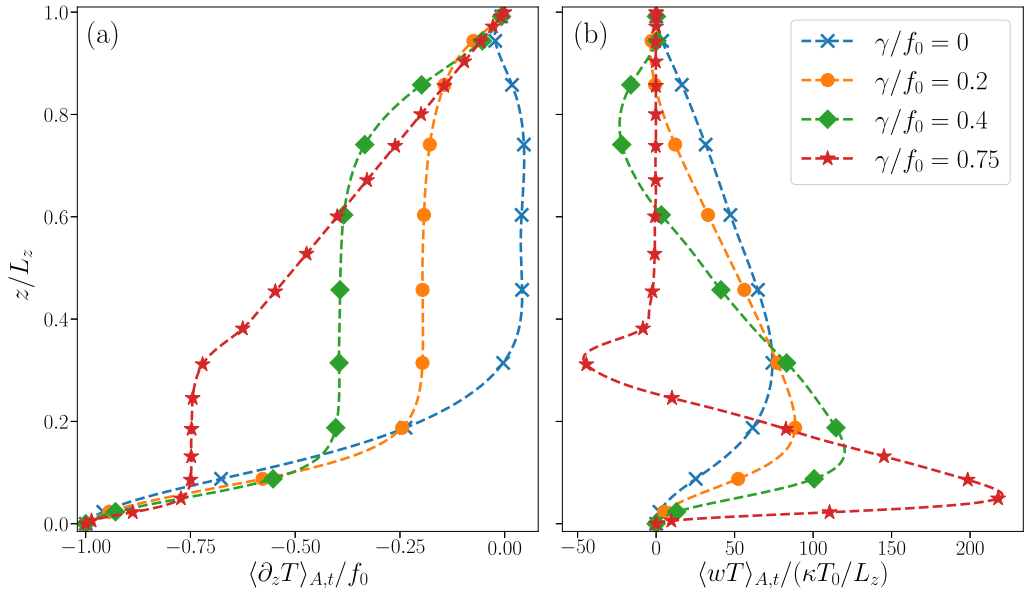

Fig. 4. (a) Average vertical profiles of $\partial_z T$ divided by f_0. (b) Average vertical profiles of wT divided by $\kappa T_0/L_z$. Both panels share the same legend, with the flows having $\mathrm{Ra}_\gamma \sim 10^4$ and the averages are statistical, height-wise averages for each flow.

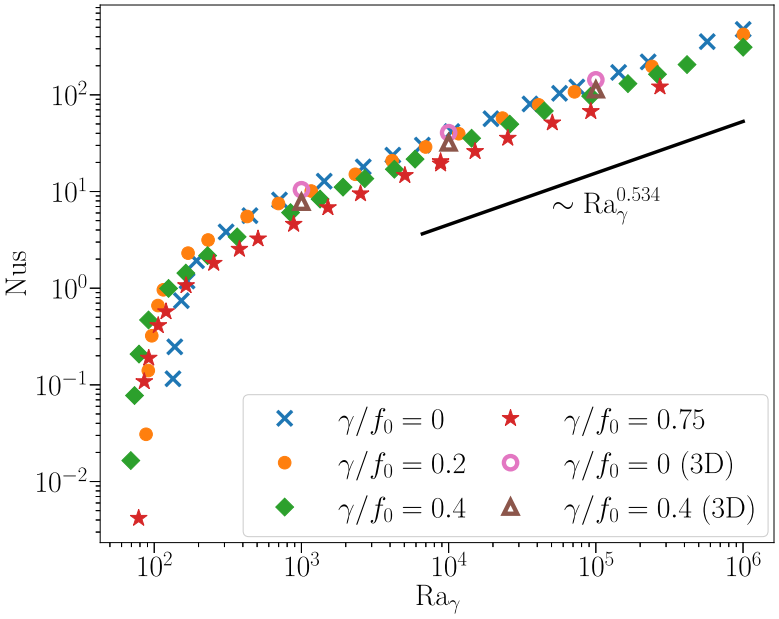

Fig. 5. Nusselt number of the flow as a function of Ra_γ for 4 different values of γ/f_0 in 2D and 2 different values in 3D.

effective mixing of the fluid ensures $\partial_z T \approx -\gamma$ up to a height of approximately z_0. For small γ, this corresponds to the top of the domain and thus there is no conducting region close to the upper boundary. Above z_0, $\partial_z T$ goes to 0 at $z = L_z$ in a linear fashion, which corresponds to the stable layer above the convective layer.

Panel (b) of Fig. 4 shows the time-averaged convective flux divided by the product of a diffusive velocity scale κ/L_z and the temperature scale T_0 - that is the height-wise Nusselt number. The convective flux attains a maxima at z roughly corresponding to the end of the lower thermal boundary layer. Above this layer and up to $z = z_0$, ie., in the convective region where $\partial_z T$ remains nearly constant, the flux decreases linearly consistent with Eq. (10).

For larger values of γ, there exists a small layer of fluid close to $z \gtrsim z_0$ where the flux is negative — this can be explained by the formation of cold patches of fluid above the rising thermal plumes. The fast rising parcels of fluid are cooled rapidly due to the lapse-rate term, leading to a region where the fluid is colder than the horizontal average while the fluid is still rising ($w > 0$),

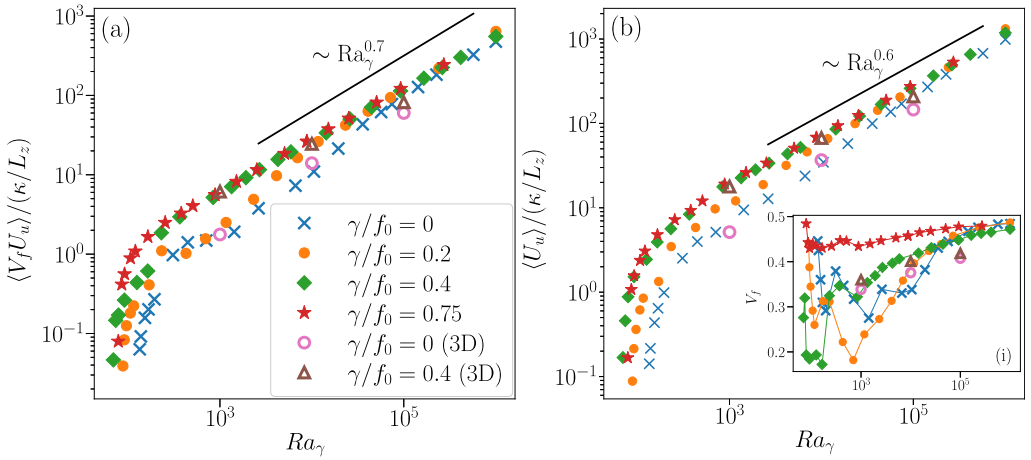

Fig. 6. (a) Domain-averaged convective mass flux plotted against Ra_γ for 4 different values of γ/f_0 in 2D and 2 values of γ/f_0 in 3D. The mass flux is non-dimensionalised by dividing it by the diffusive velocity scale κ/L_z. (b) Average velocity U_u in regions of the flow where $w > 0$ divided by the diffusive velocity scale as a function of Ra_γ for the same parameters as panel (a). Inset (i) shows the volume fraction V_f of the domain occupied by updrafts ($w > 0$).

leading to a negative flux. Above this, the fluid is no longer convecting, leading to a flux close to 0. Thus, in the presence of a large lapse-rate, the domain-averaged convective heat-flux (Nus) is partially decreased by the strong cooling of fast-rising parcels of fluid.

4.4. The Nusselt number

The convective heat-flux characterises the behavior of the flow to a large degree, as it determines the strength of the velocity and temperature gradients and also plays an import role in understanding the behavior of the fluid in the viscous boundary layers. The non dimensionalised heat-flux, the Nusselt number (defined in Eq. (13)) is thus particularly important in understanding the convective behavior of the system.

The Nusselt number is identically 0 for the conductive state as the fluid is not in motion. In the convective regime, Nus increases with increasing Ra_γ as we see in Fig. 5, which shows the scaling of the Nusselt number for changing Ra_γ and for various values of γ/f_0. For flows with identical Ra_γ, Nus is the largest for the cases with $\gamma = 0$. This is due to the fact that for flows without an imposed lapse rate, the convection is penetrative ($z_0 = L_z$) and the hot plumes reach the top of the domain. In the case of flows with a finite lapse rate, the region of the flow above z_0 contributes negatively to the total convective heat flux of the system, as already discussed in the previous section and seen in Fig. 4(b). We note that this contribution is quite small, given that the values are nearly identical for γ/f_0 ranging from 0 to 0.75. This also indicates that Ra_γ is a well-chosen parameter to characterise the large-scale behavior of this model system.

The magnitude and scaling of the Nusselt number as a function of Ra_γ for 3D flows is identical to the 2D flows. This indicates that in making estimates of dry convective heat-fluxes with given boundary conditions, it is sufficient to simulate a 2D domain.

4.5. Mass-flux, updraft velocities and up-down asymmetry

Along with the convective heat-flux, the convective mass-flux also remains an important parameter to be estimated in thermal flows, particularly in the dry atmosphere. The mass flux at a given height is calculated as the product of the volume fraction V_f of the domain which is rising ($w > 0$) and the average vertical velocity U_u within these rising regions. The total convective mass flux is the vertical average of the mass-flux at each height written as $\langle V_f U_u \rangle$.

The variation of the convective mass-flux with Ra_γ is shown in panel (a) of Fig. 6. We see that the mass flux close to the transition to convection shows large variation in magnitude depending on the value of γ/f_0, with the mass flux being greater for the flows with greater γ/f_0. For large enough Ra_γ, all values of mass-flux converge to a single line on the log–log plot, which corresponds to a power law dependence on Ra_γ with a fixed exponent. The updraft velocities U_u and the volume fraction V_f are shown in panel (b) and inset (i) respectively. For larger values of Ra_γ the values of U_u also converge to a single exponent independent of γ/f_0 while V_f converges to a single value ~ 0.48.

The variation of V_f with increasing Ra_γ with can be explained from the behavior seen in Fig. 3 - when the flow is convective and laminar (as is the case for small Ra_γ close to the critical value for transition) the only upward moving regions occur in the vicinity of the rising plume, and the entire domain is filled by a single, large convective roll. The rest of the domain is uniformly, weakly subsiding. This behavior can be observed for example on closer examination of panel (b) in Fig. 3, where a part of domain extending from approximately $x = 3$ to $x = 5.5$ is a clearly delineated upward rising region and the rest of the domain is subsiding with a much smaller velocity to compensate for the rising mass in the rising plume. For larger Ra_γ flows which are more turbulent and have greater kinetic energy, the flow contains multiple plumes and convective rolls with rapid point-wise temporal fluctuations

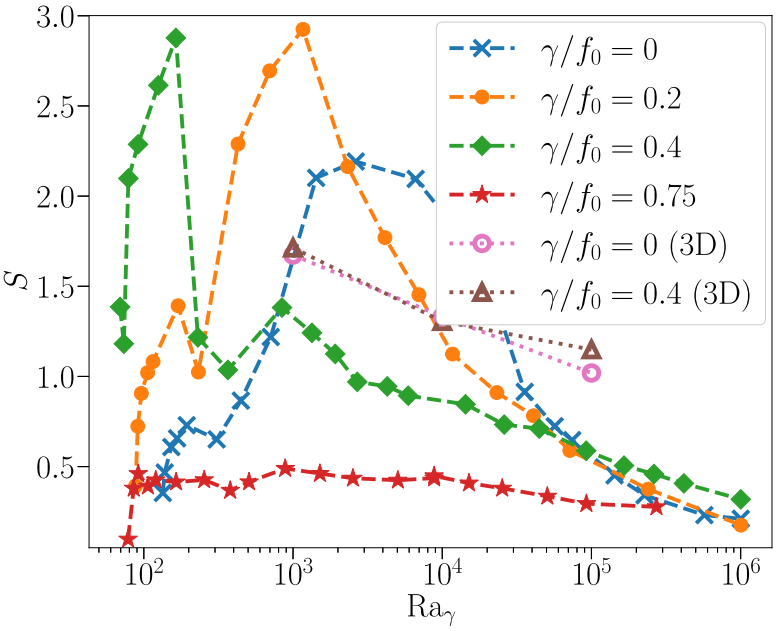

Fig. 7. Skewness S of the vertical velocity for flows with varying γ/f_0 as a function of Ra_γ for 2D and 3D simulations.

in velocity. For example, in panel (d) of the same figure, while the region between $x \approx 1$ to $x \approx 2.5$ is subsiding on average, some grid points individually have $w > 0$ within this region. For the largest values of Ra_γ, the flows are highly turbulent and energetic, leading to a V_f value close to half.

The asymmetry between up and down that results from the $-R$ term is important only in the convective region of the flow. The stable upper layer in flows with non-zero γ are locally in conductive equilibrium and fluid motion here is only due to the transport of mass and momentum from the convective region. These regions do not show an up-down asymmetry. Thus, regions with a thicker stable layer (larger γ/f_0) are overall more symmetric and the domain average V_f is closer to half, independent of Ra_γ.

The mass flux and the updraft velocity scales nearly identically in 2D as well as 3D, though in the 3D case V_f converges to a value close to half for much larger Ra_γ (if we assume that the scaling seen in Fig. 5(i) holds for larger Ra_γ). Simulations for 3D flows with $\mathrm{Ra}_\gamma > 10^5$ were not performed due to the requirement of large computing resources and are beyond the scope of this study.

While the volume fraction V_f gives an insight into the degree of asymmetry in the flow, it does not capture the relative magnitude of the velocity of rising and subsiding regions, thus does not fully quantify the asymmetry. Another measure often used (including in B2012) is the skewness measure of the vertical velocity field. The skewness S is defined as

$$S = \frac{\langle w^3 \rangle}{(\langle w^2 \rangle)^{3/2}}, \tag{48}$$

where we have used the fact that $\langle w \rangle = 0$. A positive skew implies a left-peaked distribution, where the tail on the positive end is thicker while the median w is negative. Fig. 7 shows S as a function of Ra_γ for various values of γ/f_0. S follows a trend which is close to the inverse of V_f (see Fig. 6(i)), where the value of S peaks when the value of V_f is at a minima. Similar to V_f, the skewness also converges to a value which is between 0 and 0.5 for large Ra_γ, consistent with the aforementioned small-degree of asymmetry.

It is the $-R$ term that breaks the up-down asymmetry — however we see that for greater R, the flow becomes less asymmetric. Whereas the flows with the largest degree of asymmetry have R just large enough to overcome the stabilisation by viscous forces. We note here that the key factor determining the asymmetry is the relative importance of the bulk-cooling term. Considering the non-dimensionalised heat-equation, Eq. (21), the LHS value is large when the typical magnitude of fluctuations in $\hat{T}$ and $\hat{\boldsymbol{u}}$ are large. This is the case when Ra is large. For cases of smaller and intermediate values of Ra, the magnitude of fluctuations in $\hat{T}$ and $\hat{\boldsymbol{u}}$ are small, so the cooling term is relatively more important in the dynamics.

5. Discussion and conclusions

We have presented results from 2D as well as 3D simulations of an uniformly cooled thermal fluid system in the presence of gravity and a lapse rate with a uniform heat flux at the lower surface and an adiabatic (no heat flux) boundary condition for the top surface. The fluid is assumed to be incompressible and we work in the regime of the Boussinesq approximation, which is a fair approximation for the sub-cloud layer of the earth's atmosphere, where the atmosphere is either dry or moist-unsaturated. The constant, bulk cooling term is set such that it balances the incoming heat flux at the lower surface, leading to a situation where

there is balance between a constant cooling of the domain and a heating from below, which is analogous to the atmosphere which is heated by the earth surface and constantly loses heat to space through longwave radiation. The current work is a direct extension of previous work by Berlengiero et al. reported in B2012.

The equations are non-dimensionalised using a temperature and velocity scale based on the magnitude of the diabatic cooling term. For the length-scale, we choose the height up to which the domain is unstable to dry convection z_0, where z_0 depends on the ratio between the lapse-rate γ and the uniform flux at the lower surface f_0. This leads to the lapse-rate dependent Rayleigh number denoted Ra_γ which characterises the system well. The equations are also non-dimensionalised using a diffusive velocity scaling as has been done in previous studies to give the diffusive Rayleigh number Ra_D. The two numbers are related by a simple formula, viz., $\mathrm{Ra}_D = \mathrm{Ra}_\gamma^{3/2}(1-\gamma/f_0)^{-5}$.

We show that when Ra_γ is below a critical value, conductive and viscous dissipation of heat and momentum respectively is sufficient to have a motionless steady-state solution for the fluid with all the heat transfer occurring through thermal conductivity alone. Steady-state linear stability analysis for small perturbations to this steady-state was conducted to identify the critical Ra_γ for transition from conductive state to a convective state. It was found that for small values of γ/f_0, the least stable horizontal mode has a long wavelength (wavenumber $\kappa \to 0$) and the value can be appproximated by a simple formula given in Eq. (47). For larger γ/f_0, the critical Ra_γ is given by a constant value of 78. The critical Ra_γ from 2D simulations showed an excellent match with the theoretically obtained values by solving the linear eingenvalue problem resulting from the stability analysis.

Beyond this critical value, the fluid no longer remains motionless and is unstable to small perturbations which induce a convective motion in the system. We have further shown that in this convective regime, the scaling of important measured quantities such as the Nusselt number, the non-dimensionalised mass-flux and average velocity in updrafts with Ra_γ converge to a single power-law, with some dependence of the magnitude on the dimensionless ratio γ/f_0. For large enough $\mathrm{Ra}_\gamma >\sim 10^4$, the heat-flux and the mass-flux scale as $\mathrm{Ra}_\gamma^{0.5}$ and $\mathrm{Ra}_\gamma^{0.7}$ respectively.

The bulk cooling term also introduces an up-down asymmetry in the fluid — this asymmetry is particularly marked when the flow is only weakly convective, ie. Ra_γ is only slightly larger than the critical value. For strongly convective flows, the degree of the asymmetry as measured by the volume of the domain occupied by updrafts (regions where $w > 0$) and the skewness of the vertical velocity decreases, where nearly half the domain is made up of updrafts and the skewness goes close to 0. While the 3D flows are identical to the 2D flows in the scaling of heat and mass transfers with Ra_γ, they retain a large degree of up-down asymmetry even at $\mathrm{Ra}_\gamma \sim 10^5$.

In this study, we have added to the existing body of literature on various models of thermal convective systems which help us understand atmospheric convection under different conditions. While the system has been introduced elsewhere, this is to the best of our knowledge the first study that systematically varies the parameters for a fixed-flux, internally cooled, stratified convective system, a system with particular relevance to the sub-cloud atmospheric boundary layer. Our main aim here has been to demonstrate the simple scaling of the system with respect to various input parameters and provoke future studies which explore higher Rayleigh numbers as well as mixed boundary conditions and non-uniform radiative cooling.

Idealised models of convection, including those with moisture and water phase changes serve to provide a tool to study the complex atmospheric system in a simplified setting where it is far easier to delineate the dynamic effects and feedbacks due to individual processes. In the future, we plan to study idealised models which include moist dynamics as well as global-scale idealised models which include the effects of rotation.

CRediT authorship contribution statement

Lokahith Agasthya: Conceptualization, Data curation, Formal analysis, Investigation, Methodology, Validation, Visualization, Writing – original draft, Writing – review & editing. **Caroline Jane Muller:** Conceptualization, Formal analysis, Funding acquisition, Methodology, Resources, Supervision, Validation, Writing – original draft, Writing – review & editing.

Declaration of competing interest

The authors declare that they have no known competing financial interests or personal relationships that could have appeared to influence the work reported in this paper.

Data availability

Data will be made available on request.

Acknowledgments

This project has received funding from the European Union's Horizon 2020 research and innovation programme under the Marie Sklodowska–Curie grant agreement No. 101034413. CM gratefully acknowledges funding from the European Research Council (ERC) under the European Union's Horizon 2020 research and innovation program (Project CLUSTER, Grant Agreement No. 805041). This research was supported by the Scientific Service Units (SSU) of IST Austria through resources provided by Scientific Computing (SciComp).

Appendix A. The heat-equation

We start with the first law of thermodynamics in enthalpy form given by

$$c_p \frac{DT}{Dt} - \frac{1}{\rho}\frac{Dp}{Dt} = \dot{Q} \tag{A.1}$$

where c_p is the specific heat-capacity at constant pressure and $\dot{Q}$ is the rate of diabatic heating or cooling per unit mass. We make the assumption ($D_t p \approx w\partial_z p_{ref} \approx -\rho_{ref} g w$), which is the condition of hydrostatic balance. This also assumes that a given parcel always has the same pressure as its environment, which is a common assumption made in parcel theory. This gives,

$$\partial_t T + \boldsymbol{u}\cdot\boldsymbol{\nabla}T + (g/c_p)w = \dot{Q}/c_p, \tag{A.2}$$

where the RHS includes thermal dissipation as well as diabatic cooling, which is given by $-R$ in this study. $g/c_p \equiv \gamma$ is the well known dry adiabatic lapse-rate.

Appendix B. Thermal and viscous dissipation

B.1. Thermal dissipation

The thermal dissipation is defined as

$$\epsilon_T \equiv \kappa\left\langle (\partial_i T(\boldsymbol{x},t))^2 \right\rangle_V. \tag{B.1}$$

Following [30]'s analysis for Rayleigh–Bénard convection, we multiply Eq. (3) by temperature T and average the product over the entire domain and time to give

$$\begin{aligned}\frac{1}{2}\frac{d\langle T^2\rangle}{dt} + \frac{1}{2}\left\langle \boldsymbol{u}\cdot\boldsymbol{\nabla}(T^2)\right\rangle + \gamma\left\langle wT\right\rangle + \left\langle RT\right\rangle \\ = \kappa\left\langle T\nabla^2 T\right\rangle = \kappa\left\langle \boldsymbol{\nabla}\cdot(T\boldsymbol{\nabla}T)\right\rangle - \kappa\left\langle |\boldsymbol{\nabla}T|^2\right\rangle,\end{aligned} \tag{B.2}$$

Since we working in the stationary regime, ($\partial_t\langle\cdot\rangle = 0$). Further, using the incompressibility condition (Eq. (1)) and the fluid rigid boundary condition ((4)), we get

$$\left\langle \boldsymbol{u}\cdot\boldsymbol{\nabla}(T^2)\right\rangle_V = \left\langle \boldsymbol{\nabla}\cdot(\boldsymbol{u}T^2)\right\rangle_V = 0. \tag{B.3}$$

Then, Eq. (B.2) becomes

$$\kappa\left\langle |\boldsymbol{\nabla}T|^2\right\rangle = \kappa\left\langle \boldsymbol{\nabla}\cdot(T\boldsymbol{\nabla}T)\right\rangle - \gamma\left\langle wT\right\rangle - R\left\langle T\right\rangle, \tag{B.4}$$

or

$$\epsilon_T = \kappa\left\langle \boldsymbol{\nabla}\cdot(T\boldsymbol{\nabla}T)\right\rangle - \gamma\left\langle wT\right\rangle - R\left\langle T\right\rangle. \tag{B.5}$$

Using the Gauss theorem, the first term of ϵ_T can be written in terms of a surface integral as

$$\kappa\left\langle \boldsymbol{\nabla}\cdot(T\boldsymbol{\nabla}T)\right\rangle = \frac{\kappa}{L_z}\left[\left\langle T\partial_z T\right\rangle_{z=L_z} - \left\langle T\partial_z T\right\rangle_{z=0}\right]. \tag{B.6}$$

Setting $\partial_z T|_{z=0} = -f_0$ and $\partial_z T|_{z=L_z} = -f_1 = 0$ gives the expression in Eq. (11)

$$\kappa\langle|\boldsymbol{\nabla}T|^2\rangle = \frac{\kappa}{L_z}(T_0 f_0) - \gamma\langle wT\rangle - R\langle T\rangle. \tag{B.7}$$

B.2. Viscous dissipation

Taking the dot product of Eq. (2) with $\boldsymbol{u}$ and taking the statistical average over the whole volume as above, we get

$$\begin{aligned}\frac{1}{2}\frac{d}{dt}\left\langle(\boldsymbol{u}\cdot\boldsymbol{u})\right\rangle + \frac{1}{2}\left\langle \boldsymbol{u}\cdot\boldsymbol{\nabla}(\boldsymbol{u}\cdot\boldsymbol{u})\right\rangle \\ = -\left\langle \boldsymbol{u}\cdot\boldsymbol{\nabla}p\right\rangle + \nu\left\langle \boldsymbol{u}\cdot\nabla^2\boldsymbol{u}\right\rangle + \beta g\left\langle wT\right\rangle.\end{aligned} \tag{B.8}$$

In the stationary state, the terms of the form $d_t\langle\cdot\rangle$ vanish. Using the incompressibility condition and the rigid boundary condition, we have

$$\left\langle \boldsymbol{u}\cdot\boldsymbol{\nabla}(\boldsymbol{u}\cdot\boldsymbol{u})\right\rangle_V = \left\langle \boldsymbol{\nabla}\cdot\left[\boldsymbol{u}(\boldsymbol{u}\cdot\boldsymbol{u})\right]\right\rangle_V = 0 \tag{B.9}$$

$$\langle\boldsymbol{u}\cdot\boldsymbol{\nabla}p\rangle_V = \left\langle \boldsymbol{\nabla}\cdot(\boldsymbol{u}p)\right\rangle_V = 0 \tag{B.10}$$

$$\begin{aligned}\langle \boldsymbol{u}\cdot\nabla^2\boldsymbol{u}\rangle_V &= \frac{1}{2}\left\langle \boldsymbol{\nabla}\cdot\boldsymbol{\nabla}(\boldsymbol{u}\cdot\boldsymbol{u})\right\rangle_V - \sum_{i,j}\left\langle \left(\frac{\partial u_j}{\partial x_i}\right)^2\right\rangle_V \\ &= -\sum_{i,j}\left\langle \left(\frac{\partial u_j}{\partial x_i}\right)^2\right\rangle_V \\ &= -\frac{1}{2}\sum_{i,j}\left\langle \left(\frac{\partial u_i}{\partial x_j}+\frac{\partial u_j}{\partial x_i}\right)^2\right\rangle_V .\end{aligned} \tag{B.11}$$

So, Eq. (B.8) becomes

$$\frac{\nu}{2}\sum_{i,j}\left\langle \left(\frac{\partial u_i}{\partial x_j}+\frac{\partial u_j}{\partial x_i}\right)^2\right\rangle = \beta g\langle wT\rangle, \tag{B.12}$$

or

$$\epsilon \equiv \frac{\nu}{2}\sum_{i,j}\left\langle \left(\frac{\partial u_i}{\partial x_j}+\frac{\partial u_j}{\partial x_i}\right)^2\right\rangle = \beta g\langle wT\rangle. \tag{B.13}$$

References

[1] Thomson J, et al. On a changing tesselated structure in certain liquids. Proc Phil Soc Glasgow 1882;13:464–8.
[2] Bénard H. Les tourbillons cellulaires dans une nappe liquide.-méthodes optiques d'observation et d'enregistrement. J Phys Théor Appl 1901;10(1):254–66.
[3] Rayleigh L. LIX. On convection currents in a horizontal layer of fluid, when the higher temperature is on the under side. Lond Edinb Dublin Philos Mag J Sci 1916;32(192):529–46.
[4] Ahlers G, Grossmann S, Lohse D. Heat transfer and large scale dynamics in turbulent Rayleigh-bénard convection. Rev Modern Phys 2009;81(2):503.
[5] Getling AV. Rayleigh-B nard convection: structures and dynamics, vol. 11, World Scientific; 1998.
[6] Emanuel KA. Atmospheric convection. USA: Oxford University Press; 1994.
[7] Manabe S, Smagorinsky J, Strickler RF. Simulated climatology of a general circulation model with a hydrologic cycle. Mon Weather Rev 1965;93(12):769–98.
[8] Edwards PN. History of climate modeling. Wiley Interdiscip Rev Clim Change 2011;2(1):128–39.
[9] Guichard F, Couvreux F. A short review of numerical cloud-resolving models. Tellus A: Dyn Meteorol Oceanogr 2017;69(1):1373578.
[10] Hernandez-Duenas G, Majda AJ, Smith LM, Stechmann SN. Minimal models for precipitating turbulent convection. J Fluid Mech 2013;717:576–611.
[11] Weidauer T, Schumacher J. Moist turbulent Rayleigh-bénard convection with Neumann and Dirichlet boundary conditions. Phys Fluids 2012;24(7):076604.
[12] Vallis GK, Parker DJ, Tobias SM. A simple system for moist convection: the rainy–bénard model. J Fluid Mech 2019;862:162–99.
[13] Hartlep T, Busse FH. Convection in an internally cooled fluid layer heated from below. Geophys Astrophys Fluid Dyn 2018;112(1):20–35.
[14] Berlengiero M, Emanuel K, Von Hardenberg J, Provenzale A, Spiegel E. Internally cooled convection: a fillip for philip. Commun Nonlinear Sci Numer Simul 2012;17(5):1998–2007.
[15] Goluskin D. Internally heated convection beneath a poor conductor. J Fluid Mech 2015;771:36–56.
[16] Goluskin D. Internally heated convection and Rayleigh–Bénard convection. Springer; 2016.
[17] Lepot S, Aumaître S, Gallet B. Radiative heating achieves the ultimate regime of thermal convection. Proc Natl Acad Sci 2018;115(36):8937–41.
[18] Bouillaut V, Lepot S, Aumaître S, Gallet B. Transition to the ultimate regime in a radiatively driven convection experiment. J Fluid Mech 2019;861:R5.
[19] Miquel B, Bouillaut V, Aumaître S, Gallet B. On the role of the Prandtl number in convection driven by heat sources and sinks. J Fluid Mech 2020;900:R1.
[20] Carson DJ. The development of a dry inversion-capped convectively unstable boundary layer. Q J R Meteorol Soc 1973;99(421):450–67. http://dx.doi.org/10.1002/qj.49709942105.
[21] Roberts A. An analysis of near-marginal, mildly penetrative convection with heat flux prescribed on the boundaries. J Fluid Mech 1985;158:71–93.
[22] Boussinesq J. Theorie Analytique de la Chaleur. vol. 2, Paris: Gauthier-Villars; 1903.
[23] Spiegel EA, Veronis G. On the Boussinesq approximation for a compressible fluid. Astrophys J 1960;131:442.
[24] Burns KJ, Vasil GM, Oishi JS, Lecoanet D, Brown BP. Dedalus: A flexible framework for numerical simulations with spectral methods. Phys Rev Res 2020;2(2):023068.
[25] Emanuel KA, Bister M. Moist convective velocity and buoyancy scales. J Atmos Sci 1996;53(22):3276–85.
[26] Sparrow EM, Goldstein RJ, Jonsson V. Thermal instability in a horizontal fluid layer: effect of boundary conditions and non-linear temperature profile. J Fluid Mech 1964;18(4):513–28.
[27] Chandrasekhar S. Hydrodynamic and hydromagnetic stability. Courier Corporation; 2013.
[28] Choi C, Kim J, Hwang S. The stability of a fluid layer heated uniformly from below. Korean J Chem Eng 1985;2:17–23.
[29] Depassier M, Spiegel E. The large-scale structure of compressible convection. Astron J 1981;86:496–512.
[30] Siggia ED. High Rayleigh number convection. Annu Rev Fluid Mech 1994;26(1):137–68.